Short- and medium-range order in $(Zr_{70}Cu_{20}Ni_{10})_{90-x}Ta_xAl_{10}$ bulk amorphous alloys

T. C. Hufnagel*
Department of Materials Science and Engineering, Johns Hopkins University, Baltimore, Maryland 21218-2681

S. Brennan
Stanford Synchrotron Radiation Laboratory, Menlo Park, California 94025

(Received 13 August 2002; published 22 January 2003)

We have used x-ray scattering to examine short-range and medium-range order in $(Zr_{70}Cu_{20}Ni_{10})_{90-x}Ta_xAl_{10}$ amorphous alloys. Analysis of the radial distribution functions (RDF's) shows that the addition of 4 at. % Ta enhances the average short-range topological order, as the nearest-neighbor peak in the RDF becomes more sharply defined. The enhanced order due to the Ta addition persists beyond the first few atomic shells, however, out to distances of at least 15 Å. From resonant x-ray scattering near the Zr *K* absorption edge, we are able to extract differential radial distribution functions (DRDF's) which show the atomic environment around Zr atoms only. The DRDF's show that Ta has little effect on the nearest neighbors of Zr atoms, but does significantly enhance the medium-range order (over distances of 5–15 Å from an average Zr atom). To explain these observations, we propose that topologically ordered atomic clusters are a significant feature of the structure of Zr-based amorphous alloys and that the influence of Ta is to enhance the order associated with packing of these clusters.

DOI: 10.1103/PhysRevB.67.014203 PACS number(s): 61.43.−j, 81.05.Kf, 61.10.Eq

I. INTRODUCTION

Over the past decade, there has been renewed interest in the properties of metallic glasses, prompted largely by the development of multicomponent bulk glass-forming alloys which can be made in sufficiently large sizes to allow their use in structural applications.[1,2] In particular, the widespread availability of bulk specimens (as opposed to ribbons produced by rapid solidification) has made possible a wide range of studies of the mechanical behavior of amorphous alloys, which has led to a dramatic improvement in our understanding of fundamental aspects of deformation and fracture.[3–13]

Our understanding of the structure of amorphous alloys, however, has not advanced nearly so rapidly. There are several reasons for this. First, the microstructure (which we loosely define as structure with characteristic length scales of 2 nm to 0.1 mm) of amorphous alloys, such as phase separation into compositionally distinct amorphous phases, is much more subtle than that of crystalline alloys which have easily observable features such as grain boundaries and second-phase particles. Second, characterizing the short-range order (0–0.5 nm) of an amorphous alloy is quite difficult with present techniques, particularly for multicomponent alloys which have $n(n+1)/2$ independent pair correlations (where n is the number of components). Third, structure over intermediate-length scales (0.5–2 nm), commonly called ''medium-range order,'' is also difficult to adequately characterize with scattering techniques (which are only sensitive to pair correlations), although some progress has been made recently in using fluctuation microscopy to characterize these length scales in amorphous materials.[14,15] Finally, although computer simulations of disordered structures have great promise, accurate simulation of multicomponent ($n>2$) systems remains quite difficult.[16] Despite these difficulties, it is clear that structure-property relationships are central to the behavior of amorphous materials, just as they are in crystalline materials, and that our understanding of these relationships is limited by our lack of detailed information on the structure of metallic glasses.

We report here on the effect of alloy content on the structure of $(Zr_{70}Cu_{20}Ni_{10})_{90-x}Ta_xAl_{10}$ bulk amorphous alloys. (All compositions are reported in atomic percent.) These alloys are of interest because the addition of small concentrations of Ta ($x\leqslant 5\%$) has a significant effect on the mechanical behavior of the material, increasing the plastic strain to failure observed in uniaxial compression, apparently through an influence on the propagation of shear bands.[17] Preliminary fluctuation microscopy studies indicate that the Ta-containing alloys have enhanced medium-range order relative to alloys without Ta.[15] In the present work, we have employed x-ray scattering techniques (including resonant scattering at the Zr *K* absorption edge) to examine the short-range and medium-range order of alloys with ($x=4$) and without ($x=0$) Ta. We find that the primary effect of Ta is to enhance the structural order in the second-nearest-neighbor shells around Zr atoms. We propose that this structural order is associated with topologically ordered clusters in the amorphous alloy and that the enhanced medium-range order of the Ta-containing alloys is due to stronger ordering between clusters.

II. EXPERIMENT

A. Sample preparation

Samples of amorphous $(Zr_{70}Cu_{20}Ni_{10})_{90-x}Ta_xAl_{10}$ with $x=0$ and $x=4$ were produced by arc melting master alloy ingots of the desired composition and casting into a copper mold to produce ingots 3 mm diameter and approximately 75 mm long. The master alloy ingots were prepared by arc melting high-purity elemental metals under a Ti-gettered Ar atmosphere. To ensure even distribution of the alloying ele-

ments, the alloy ingots were remelted several times. Samples 25 mm long, 2 mm wide, and 1 mm thick for x-ray scattering were cut from the cylindrical amorphous rods, and the surface to be examined was mechanically polished with an alumina slurry to remove any contaminated or damaged surface layer.

B. X-ray scattering

We performed the x-ray scattering experiments on beamline 10-2 at the Stanford Synchrotron Radiation Laboratory (SSRL). We made scattering measurements in a symmetric reflection geometry at x-ray energies 10 eV and 100 eV below the Zr *K* absorption edge (17 998 eV). Scattering near an absorption edge gives rise to several inelastic scattering processes as well as the desired elastic scattering signal. In order to discriminate the elastic scattering, we used a sagitally focusing graphite analyzer crystal in the scattered beam, which focused the scattered radiation onto a position-sensitive detector. The analyzer-detector system, which is described in more detail elsewhere,[18] had an energy resolution of 50 eV (0.3%) at the Zr *K* edge. Systematic errors were minimized by collecting multiple x-ray scattering patterns from each sample at each x-ray energy in a single run and averaging the results. Variations in the incident beam intensity were monitored by means of an ion chamber upstream of the sample; the elastic scattering intensity was normalized to this ion chamber reading.

The atomic scattering factor for an element is quite sensitive to the x-ray energy at energies close to an absorption edge of that element. Therefore, it is critical to pay attention to the reproducibility with which the incident x-ray energy is selected from the white synchrotron radiation. For instance, small changes in the position of the orbiting electron beam or small instabilities in the monochromator system (due to beam heating, for instance) can cause shifts of several eV in the incident x-ray energy, which is enough to significantly affect the results. To minimize this problem, we checked the x-ray energy of the incident beam frequently (typically after every scan), by measuring the absorption through a foil of the element of interest (Zr here) as a function of x-ray energy and locating the absorption edge. The energy for subsequent scans was then defined relative to the position of the absorption edge. In this way, we achieve reproducibility in the x-ray energy for our scattering scans of better than 1 eV.

To extract structural information, we corrected the elastically scattered intensity $I(q)$ for the effects of detector dead time, absorption, multiple scattering, and polarization of the incident beam; the corrections are standard procedures that are described in detail elsewhere.[19] The resulting scattering data are in arbitrary units; to place them on an absolute scale, we normalized them to the coherent independent scattering intensity using the method of Norman and Krogh-Moe[20,21] and scattering factors tabulated by Kissel *et al.*[22,23] From the normalized scattering intensity $I(q)$ in electron units, we calculated the total structure factor $S(q)$, defined as

$$S(q) \equiv \frac{I(q) - \langle f^2 \rangle}{\langle f \rangle^2}, \tag{1}$$

where f is the atomic scattering factor and the brackets indicate an average over all elements, weighted according to the composition of the specimen. The real-space structural information available from $S(q)$ is called the radial distribution function (RDF), defined as

$$4\pi r^2 \rho(r) = 4\pi r^2 \rho_0 + \frac{2r}{\pi} \int_0^\infty qS(q)\sin(qr)dq. \tag{2}$$

In this equation, $\rho(r)$ is the atomic density at a distance r from a compositionally averaged atom and ρ_0 is the average atomic density of the specimen. Because $S(q) \to 0$ as r becomes large, the radial distribution function only shows significant structure for the first few atomic shells surrounding an average atom. It is also sometimes convenient to work with the reduced radial distribution function (RRDF), which is simply the RDF with the average atomic density term subtracted:

$$4\pi r^2 [\rho(r) - \rho_0] = \frac{2r}{\pi} \int_0^\infty qS(q)\sin(qr)dq. \tag{3}$$

C. Angular dependence of the anomalous scattering factors

The energy dependence of the atomic scattering factor $f(q,E)$ is commonly written as

$$f(q,E) = f_0(q) + f'(q,E) + if''(q,E), \tag{4}$$

where $f_0(q)$ is the atomic form factor, E is the x-ray energy, and $f'(q,E)$ and $f''(q,E)$ are the anomalous scattering factors. Although there are several tabulations of anomalous scattering factors as a function of x-ray energy available,[22–25] these tabulations are of insufficient accuracy for scattering experiments performed very close to an absorption edge. Therefore, when performing resonant scattering experiments, one must measure f' and f'' for the samples being studied. This can be conveniently accomplished by measuring the x-ray absorption through a thin specimen, calculating f'' from the absorption using the optical theorem, and then calculating f' from f'' using the Kramers-Kronig transformation.[26] We did this to determine f' and f'' for Zr, from absorption measurements around the Zr *K* absorption edges; the results are presented in Table I. Notice that the measured values differ significantly from the tabulated values at energies close to the absorption edge.

In Eq. (4), the form factor is presumed to be independent of x-ray energy; the energy dependence of f is ascribed solely to the anomalous scattering factors. Although in general the anomalous scattering factors are also functions of the scattering angle (through their dependence on q), it is common to use the forward scattering ($q=0$) values for f' and f'' and assume that they are independent of scattering angle. In most resonant scattering work performed to date, the angle-independent approximation has been adequate. Recent work has shown, however, that the angular dependence of the anomalous scattering factors can be significant.[27] In the present case, we have found a discrepancy in the normalization of our scattering very close to the Zr *K* edge, which

TABLE I. Comparison of the experimentally determined anomalous scattering factors for Zr below the Zr *K* absorption edge (which is at 17998 eV), with calculations of Cromer and Liberman (Ref. 24), Henke *et al.* (Ref. 25), and Kissel *et al.* (Ref. 22). Kissel's self-consistent calculations yield absorption edge energies that are different from those experimentally observed, so in using them to calculate the anomalous scattering factors below, the energy was rescaled to yield the proper energy with respect to the position of the absorption edge.

	$E=17898$ eV		$E=17988$ eV	
	f'_{Zr}	f''_{Zr}	f'_{Zr}	f''_{Zr}
Measured	−4.38	0.55	−7.13	0.88
Cromer-Liberman	−4.52	0.54	−6.87	0.53
Kissel *et al.*	−4.38	0.55	−7.56	0.54
Henke *et al.*	−5.03	0.56	−10.29	0.55

leads us to conclude that, in this case at least, it is important to take account of the angular dependence of f' and f''.

Because the experimental data are on an arbitrary scale, calculating $S(q)$ involves finding a normalization constant that makes $I(q)$ oscillate smoothly about the independent coherent scattering $\langle f^2\rangle$. As Eq. (1) indicates, for properly normalized data $S(q)$ will oscillate about zero at large q. This is the case for the data recorded 100 eV below the Zr *K* edge as well as additional data collected near the Ta L_{III} edge (not shown). Indeed, the excellent energy resolution of the analyzer crystal, which essentially eliminates all of the inelastic scattering, makes normalization of those data quite straightforward. Figure 1(a), however, shows the total structure factor $S(q)$ calculated from the elastic scattering $I(q)$ measured 10 eV below the Zr *K* absorption edge, using Eq. (1) and assuming that the anomalous scattering factors are independent of scattering angle. Notice that $S(q)$ does not oscillate about zero and that there is a monotonic increase in $S(q)$ at large q for both specimens. We carefully considered possible systematic errors in the experiment that might be responsible for these features, but were unable to adequately account for them. Many sources of error can be discounted because our detector counts only elastic scattering (eliminating inelastic scattering processes from consideration) and because data from the same sample, recorded at nearly the same time at an x-ray energy, only 90 eV lower, do not show similar effects.

On the basis of these considerations, we concluded that the most likely source of the problems in Fig. 1 was some inaccuracy in the anomalous scattering factors. However, we were also unable to achieve a well-behaved $S(q)$ by any choice of angle-independent anomalous scattering factors for Zr. Therefore, we considered whether assuming an angular dependence would yield well-behaved total structure functions. In particular, we adopted the following form for f':

$$f'(\theta,E)=f'(0,E)[1+a'_1\sin^2\theta+a'_2\sin^4\theta], \qquad (5)$$

where $f'(0,E)$ is the measured value of f' in the forward-scattering direction and the coefficients a'_1 and a'_2 determine the angular dependence of f'.[23,28] A similar expression may be written for f'' (with coefficients a''_1 and a''_2), but because f'' is small in comparison to f' for scattering below the *K* edge (Table I), we elected to continue to assume that f'' was independent of scattering angle. Having measured f' for forward scattering only, we had no independent basis for choosing a'_1 and a'_2, so we selected values that gave a well-behaved $S(q)$ for the 0% Ta specimen. When we applied the same values of a'_1 and a'_2 to the other (4% Ta) specimen, they yielded a similarly well-behaved $S(q)$. The fact that the same choice of coefficients gives good results for two specimens of different composition makes us confident that it is indeed this angular dependence that caused the discrepancies in Fig. 1(a). In making final choices for a'_1 and a'_2, we made slight adjustments that optimized the overall behavior of $S(q)$ for both specimens, as shown in Fig. 1(b). The final values were $a'_1=-0.10$ and $a'_2=-0.28$.

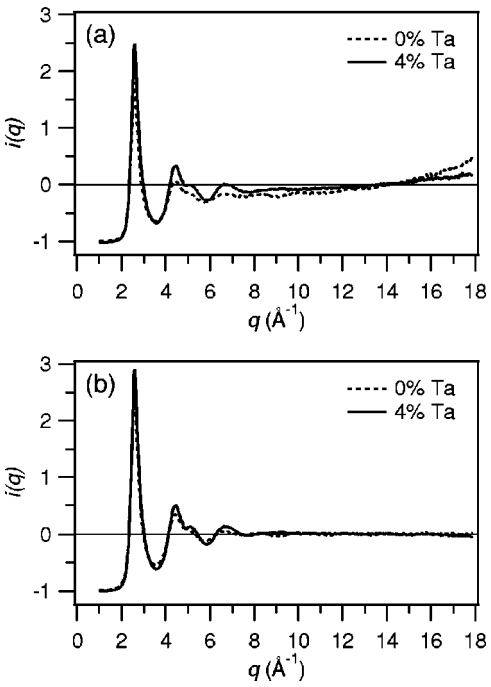

FIG. 1. (a) Total structure functions $S(q)$ for $(Zr_{70}Cu_{20}Ni_{10})_{90-x}Ta_xAl_{10}$ with $x=0$ and $x=4$, from scattering data taken with an x-ray energy of 17988 eV (10 eV below the Zr *K* absorption edge), assuming angle-independent anomalous scattering factors. The normalization was done using the method of Norman and Krogh-Moe, with an integral over the entire range of q (Refs. 20 and 21). (b) Total structure functions $S(q)$ calculated from the same data as (a), but using angle-dependent f'. The same coefficients a'_1 and a'_2 were used in normalizing the data from both specimens.

III. RESULTS

A. Average atomic environments

Figure 2(a) shows the low-r region of the radial distribution functions, calculated from scattering data taken at an x-ray energy of 17898 eV (100 eV below the Zr *K* edge), for both specimens (0% and 4% Ta). The first-nearest-neighbor peak is at $r\simeq 3.1$ Å, and the coordination number (obtained

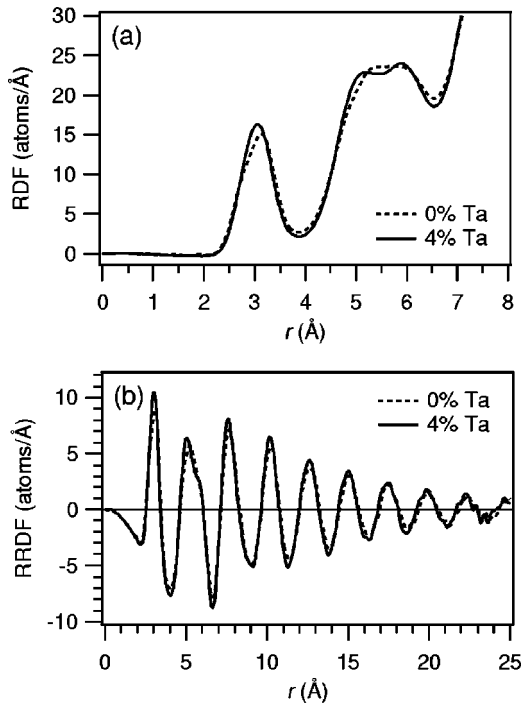

FIG. 2. (a) Radial distribution functions $[4\pi r^2\rho(r)]$ for $(Zr_{70}Cu_{20}Ni_{10})_{90-x}Ta_xAl_{10}$ with $x=0$ and $x=4$. (b) Reduced radial distribution functions $(4\pi r^2[\rho(r)-\rho_0])$ for the same samples as in (a).

by integrating the area under the peak) is 12.1 ± 0.9 for both compositions. The peak is slightly sharper for the 4% Ta alloy, with a full width at half maximum of 0.74 Å, compared to 0.80 Å for the 0% Ta alloy, suggesting that the topological short-range order is slightly stronger for the 4% Ta alloy.

Because the radial distribution function reveals the atomic environment around a hypothetical average atom, the first-nearest-neighbor peak has contributions from all of the unique atomic pairs. For a four-component alloy (0% Ta) there are 10 such partial pair correlations, while there are 15 for a five component alloy (4% Ta). Determining all of the partial pair correlations is, at present, an intractable problem for amorphous alloys of this complexity. We can, however, make some general statements regarding the short-range order in these alloys. The prominent peak in the RDF's near $r\simeq3.1$ Å is due to Zr-Zr pair correlations; this conclusion is supported by the resonant scattering results (described below) as well as earlier work on Zr-rich ternary amorphous alloys.[29,30] There is another peak in the RDF, visible at $r\simeq2.8$ Å as a shoulder on the main peak. This peak is due primarily to Zr-Cu and Zr-Ni pair correlations; there may also be Cu-Cu and Ni-Ni pairs, but these are expected to be uncommon.[29] The influence of Ta on the nearest-neighbor environment is seen for the 4% Ta alloy as an increase in amplitude of the first peak in the RDF; since the atomic radius of Ta (1.45 Å) is slightly smaller than that of Zr (1.55 Å),[31] the peak maximum shifts to slightly lower r. Despite the increase in amplitude, the average coordination number is unchanged, because the peak is also slightly sharper for the 4% Ta alloy, making the area under the first peak the same for the two alloys. Finally, no conclusions can be drawn regarding Al, because the scattering factor of Al is small, and it is present at a relatively low concentration, making it essentially undetectable in these experiments.

To extract more quantitative information about these pair correlations, we fit a model consisting of three Gaussian profiles to the nearest-neighbor peaks in the RDF's. Two of the Gaussian profiles represented pair correlations, while the third was used to represent the overlap from the second-nearest-neighbor peak. The results are shown in Table II. The pair separations and coordination numbers obtained in this way are in good agreement with similar measurements on ternary alloys.[29] The only significant difference between the two alloys is the shift of the second peak from $r=3.14$ Å (0% Ta) to $r=3.07$ Å (4% Ta), consistent with the existence of pair correlations involving Ta. The greatest increase in the amplitude of the RDF occurs around $r=2.8$–2.9 Å, suggesting that the Ta is strongly coordinated with Ni, Cu, or both. There are also some small changes in the partial coordination numbers, but these are probably not statistically significant, due to the extensive overlap between the two peaks.

The second-nearest neighbor peak in the RDFs occurs at $r\simeq5$–6 Å. As is common for amorphous alloys, the second peak shows some splitting corresponding to two different pair separations. This splitting is more prominent for the 4% Ta alloy than the 0% Ta alloy. The structure at larger r is more easily seen by examining the reduced radial distribution function. The RRDF's for the two alloys are shown in Fig. 2(b); because the average atomic density term has been

TABLE II. Pair separations (r), coordination numbers (CN's), and peak widths (w) determined from the RDF's by fitting the first-nearest-neighbor peak to a sum of two Gaussian peaks representing the pair correlations. The uncertainties reported represent one standard deviation from the best-fit parameters. The first peak is primarily due to Zr-Ni and Zr-Cu pair correlations, while the second is primarily due to Zr-Zr correlations and, in the 4% Ta alloy, correlations involving Ta. Note, however, that there is considerable overlap of the peaks. The total coordination number of the first-nearest-neighbor shell is 12.1 ± 0.9 for both alloys.

	Peak 1 (primarily Zr-Ni and Zr-Cu)			Peak 2 (primarily Zr-Zr and Zr-Ta)		
	r (Å)	Area (atoms)	Width (Å)	r (Å)	Area (atoms)	Width (Å)
0% Ta	2.68 ± 0.02	1.9 ± 1.0	0.35 ± 0.03	3.14 ± 0.01	10.2 ± 0.4	0.62 ± 0.02
4% Ta	2.67 ± 0.03	0.5 ± 0.8	0.25 ± 0.07	3.07 ± 0.01	11.6 ± 0.4	0.65 ± 0.01

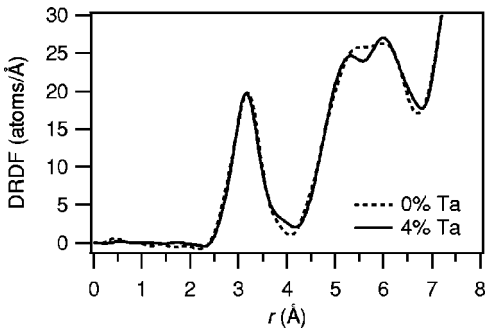

FIG. 3. Differential radial distribution functions calculated from scattering data collected at x-ray energies 10 eV and 100 eV below the Zr *K* absorption edge for $(Zr_{70}Cu_{20}Ni_{10})_{90-x}Ta_xAl_{10}$ with $x=0$ and $x=4$. The differential radial distribution function shows the average atomic environment around Zr atoms.

subtracted, the RRDF's oscillate about zero. Although the RRDF's from the two alloys are similar, there is a significant difference in that the amplitude of the peaks is always greater for the 4% Ta alloy than the 0% Ta alloy. This difference persists out to relatively large distances of $r \simeq 15$ Å. In addition, the peaks in the RRDF for the 4% Ta alloy for $r > 7$ Å are shifted to slightly lower r relative to those for the 0% Ta alloy. This observation suggests slightly more efficient atomic packing for the 4% Ta alloy, as discussed below.

B. Atomic environment around Zr atoms

Although it is very difficult to extract all of the partial pair correlation functions for a multicomponent alloy from x-ray scattering data, there are some approaches that can yield some useful information. One is to make use of the fact that, at x-ray energies near an absorption edge of an element in a sample, only the scattering factor of that element changes significantly with energy. If we collect scattering data at two energies near an absorption edge, to a reasonable approximation the difference between the two sets of scattering data will reflect only pair correlations that involve the element under consideration. This approach is called differential resonant (or anomalous) scattering,[32] and it has been profitably applied to the study of binary and multicomponent amorphous alloy systems.[29,33,34]

We have used differential resonant scattering to study our samples by collecting x-ray scattering data at energies 10 eV and 100 eV below the Zr *K* absorption edge. The resulting structural information takes the form of a differential radial distribution function (DRDF), which shows the atomic environment around Zr atoms (only). The DRDF thus resembles the information available from x-ray absorption spectroscopy (XAS). For our purposes, however, an important advantage of resonant x-ray scattering is that it gives reliable information at low q, which in turn yields more reliable information than XAS about structure beyond the first-nearest-neighbor shell in amorphous materials.

Figure 3 shows the differential radial distribution functions for both alloys. In this case, we can definitely ascribe the first peak in the DRDF's to overlapping Zr-Zr, Zr-Cu, and Zr-Ni pair correlations (in addition to possible Zr-Ta pairs for the Ta-containing alloy). Results of a similar peak-fitting procedure to that used with the RDF's are presented in Table III. For the 4% Ta alloy, it was necessary to incorporate an additional Gaussian profile to adequately fit the region around $r=4$ Å. This peak occurred at a large r of 3.79 Å, which is probably too large to represent a pair correlation. It is possible that this peak is due to an unusual topological arrangement around the central Zr atom, but it is more likely that it is simply an artifact. (The DRDF's are, in general, not as reliable as the RDF's due to the error associated with calculating a small difference between two scattering measurements.)

It is apparent from Fig. 3 and Table III that the addition of Ta has only a minor effect on the nearest-neighbor environment around Zr atoms. There is a slight shift of the peak, but the changes are small compared to those seen in the radial distribution functions [Fig. 2(a)], suggesting that there are relatively few Zr-Ta nearest-neighbor pairs and that Ta has little effect on the short-range order around Zr atoms. (Even though Ta is present at a low concentration, its scattering factor is so large relative to the other elements that even a small number of Zr-Ta nearest-neighbor pairs would be discernible in the DRDF, much as the effect of Ta can be seen in the RDF.) Interestingly, however, the effect of Ta on the second-near-neighbor peak ($r \simeq 5-6$ Å) is, if anything, even more significant in the DRDF's than in the RDF's (Fig. 4). Thus, it appears that the addition of Ta enhances the structural order around Zr atoms beyond the first-nearest-neighbor shell, even though it does not change the short-range order significantly.

C. Atomic density

We measured the mass density of both samples by Archimede's method; the results are shown in Table IV.

TABLE III. Pair separations (r), coordination numbers (CN's), and peak widths (w) determined from the Zr edge DRDF's by fitting the first-nearest-neighbor peak to a sum of Gaussian peaks representing the pair correlations. The uncertainties reported represent one standard deviation from the best-fit parameters. For the 0% Ta alloy, two Gaussian peaks were sufficient, but for the 4% Ta alloy a third Gaussian was required to adequately fit the region around $r=4$ Å (see Fig. 3). The coordination number around Zr atoms is 14.0 ± 0.7 for the 0% Ta alloy and 14.3 ± 0.5 for the 4% Ta alloy.

	Peak 1 (primarily Zr-Cu and Zr-Ni)			Peak 2 (primarily Zr-Zr and Zr-Ta)			Peak 3		
	r (Å)	CN (atoms)	w (Å)	r (Å)	CN (atoms)	w (Å)	r (Å)	CN (atoms)	w (Å)
0% Ta	2.72 ± 0.02	0.7 ± 0.6	0.22 ± 0.03	3.18 ± 0.01	13.3 ± 0.3	0.63 ± 0.01			
4% Ta	2.71 ± 0.02	0.4 ± 0.3	0.23 ± 0.03	3.16 ± 0.01	12.2 ± 0.4	0.57 ± 0.01	3.79 ± 0.02	1.7 ± 0.2	0.52 ± 0.04

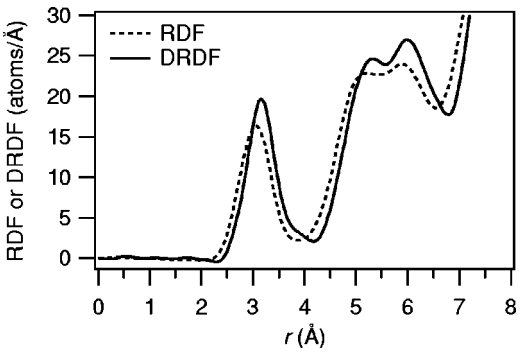

FIG. 4. Comparison of radial distribution function (RDF) and Zr edge differential radial distribution function (DRDF) for the 4% Ta alloy. Notice that the nearest-neighbor peak of the DRDF is slightly sharpened and shifted to larger r relative to the RDF; this is because the DRDF excludes all pair correlations not involving Zr (which is the largest atom in the alloy). Also notice the differences in the second-nearest-neighbor shell.

From the mass density and the composition of the samples, the atomic densities can be calculated. Based on this calculation, the 4% Ta alloy has an atomic density 1.3% larger than the 0% Ta alloy.

This difference in atomic density can also be confirmed from the x-ray scattering data, in two ways. As discussed above, the peaks representing atomic shells in the RRDF [Fig. 2(b)] from the 4% Ta sample are shifted to slightly smaller r, relative to the 0% Ta sample. The number of atoms in each shell is essentially the same for each sample (as determined by integration of the area under the peaks in the RDF), so the smaller spacing for the 4% Ta alloy indicates a higher atomic density for that sample. The fractional difference in atomic density $\Delta\rho_0/\rho_0$ is related to the fractional difference in the radii of the atomic shells $\Delta r/r$ by

$$\frac{\Delta r}{r}=\left(\frac{\Delta\rho_0}{\rho_0}+1\right)^{1/3}-1, \tag{6}$$

so we can determine $\Delta\rho_0/\rho_0$ from the slope of a plot of Δr against r. Such a plot is presented in Fig. 5(a). The calculated difference in atomic density is 1.4%, in good agreement with the calculation based on the mass density.

The second way to confirm the difference in atomic density is from the behavior of the RRDF at low r [Eq. (3)]. Because $\rho(r)=0$ below the first-nearest-neighbor shell, the slope of a plot of the RRDF against r^2 at small r is $-4\pi\rho_0$, as shown in Fig. 5(b). The difference in atomic density measured in this way is 3.7% (Table IV), somewhat larger than that from the other two methods. The discrepancy is likely due to oscillations in the RRDF for the 4% Ta alloy at low r, which make accurate determination of the slope difficult.

TABLE IV. Atomic density ρ_0 of the two alloys, determined from the measured mass density ρ_m and from the RRDF, as described in the text.

	ρ_m (g cm^{-3})	ρ_0 (Å^{-3}) (from ρ_m)	ρ_0 (Å^{-3}) (from RRDF)
0% Ta	6.587±0.004	0.05160±0.0005	0.052±0.01
4% Ta	7.008±0.004	0.05227±0.0005	0.054±0.01

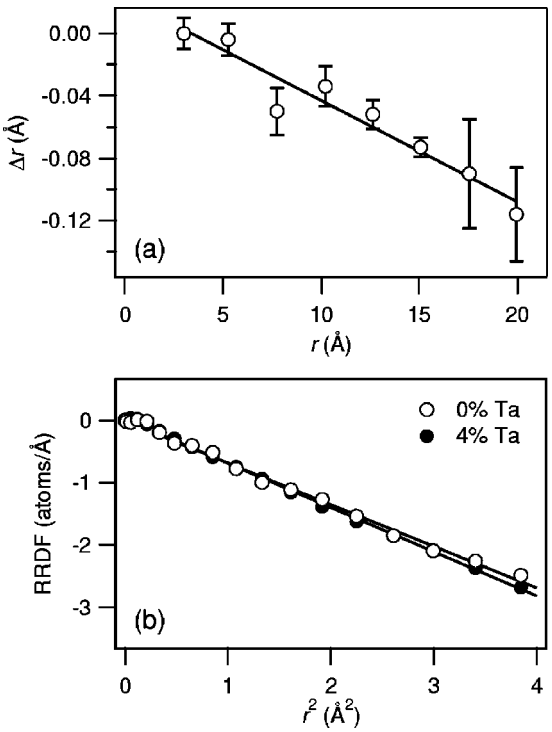

FIG. 5. (a) Plot of the difference in the positions of atomic shells (from the RRDF's) between the 0% and 4% Ta alloys. The atomic shells are shifted to lower r for the 4% Ta alloy, indicating greater atomic density. The line is a least-squares fit to the data; the slope of the line is related to the difference in atomic density of the two alloys, as discussed in the text. (b) Plot of the RRDF's against r^2. (For clarity, only every third datum is shown.) In the low r, the slope of this plot is proportional to the atomic density of the material.

IV. DISCUSSION

It is clear from the preceding discussion that the 4% Ta alloy has slightly higher atomic density than the 0% Ta alloy. The easiest way to understand this behavior is simply to imagine that when Ta is added to the alloy, the Ta atoms replace other atoms in the amorphous structure. Since the atomic volume of Ta is slightly smaller than that of Zr, it is reasonable to suppose that such a substitution would result in an increase in atomic density of the material. A simple calculation, treating the atoms as hard spheres and using the neutral atom radii,[31] suggests that on going from $Zr_{63}Cu_{18}Ni_9Al_{10}$ ($x=0$) to $Zr_{59}Cu_{17}Ni_9Ta_4Al_{10}$ ($x=4$) a 1.8% increase in atomic density should be expected solely on the basis of this atomic size difference. This prediction is in reasonably good agreement with the measured difference in atomic density.

It is clear, however, that the addition of Ta in these alloys does have an effect on the structure. In particular, there is increased structural order over length scales of 5–15 Å. This

increased structural order is either not accompanied by a significant increase in atomic density (since the prediction based solely on atomic size matches the experimental observation) or, more likely, any increase in density due to enhanced order is smaller than the atomic size effect.

One approach to understanding the structure of amorphous alloys is to match the features observed in radial distribution functions (or total structure functions) with predictions obtained from models based on various atomic packing geometries. This approach has had some important successes, notably the demonstration that the splitting of the second peak in the RDF is inconsistent with microcrystalline models of atomic-scale structure.[35] More accurate models of the structure of metals glasses are based on packing of spheres, either randomly or into short-range clusters of various topologies,[36] including icosahedral clusters,[37] with additional disordered material in the regions between clusters. Even in the case of dense random packing, some atomic geometries (referred to as ''canonical holes'') occur frequently, and it is clear that the short-range order is not really random. In what follows, we describe the structure of our glasses in terms of this short-range order. It should be understood that scattering techniques have an inherent limitation in their ability to discriminate among various models, as they only provide information about average atomic pair separations and coordination numbers. In many cases, what is required is information about bond angles, which is not available from a scattering experiment. Thus, even if there was a single dominant packing geometry, in general it would not be possible to uniquely identify it using scattering techniques alone. We can, however, make some general statements regarding the structural order.

Addition of Ta to $(Zr_{70}Cu_{20}Ni_{10})_{90-x}Ta_xAl_{10}$ has little effect on the nearest-neighbor environment around Zr atoms (Fig. 3), suggesting that there are relatively few Zr-Ta nearest neighbors. The fact that Ta is not strongly coordinated by Zr is also supported by the lack of a ''prepeak'' in the structure factor [Fig. 1(b)], which is sometime observed when a heavy element is coordinated by a lighter element in an amorphous alloy.[34] This observation is consistent with some simple predictions based on solution thermodynamics. Zr and Ta have a small positive heat of mixing, which opposes the formation of Zr-Ta nearest-neighbor pairs. In contrast, Zr has a large negative heat of mixing with the other elements in the alloy, which promotes the formation of Zr-Ni, Zr-Cu, and Zr-Al nearest-neighbor pairs. Furthermore, the alloys are Zr rich, so there are bound to be a relatively large number of Zr-Zr pairs. This picture of the Zr nearest-neighbor environment is consistent with the most detailed structural studies of Zr-rich ternary metallic glasses available.[29,30] If there are few Zr-Ta nearest-neighbor pairs, then Ta must be associated with other elements. The most likely candidates are Ni and Al, both of which have a negative heat of mixing with Ta. The existence of Ta-Ni and Ta-Al near-neighbor pairs would be consistent with the changes in the first peak in the RDF associated with the addition of Ta (Fig. 2).

Based on this simple picture of the Zr nearest-neighbor environment, one can imagine that the predominant short-range order in these alloys is a cluster consisting of a central Zr atom coordinated by other Zr atoms and some or all of Cu, Ni, and Al (Fig. 6). The Ni and Al, in turn, may have one or more Ta atoms as nearest neighbors. One effect of Ta is to enhance the ordering in the second peak in the DRDF (Fig. 3), which in our model would be the shell surrounding the cluster. Exactly how Ta does this is not clear, but it may be related to the fact that Ta atoms are intermediate in size between Zr and either Cu or Ni, which may promote more efficient atomic packing, or to chemical ordering associated with the negative heat of mixing of Ta with Ni and Al. We suspect, though, that each Ta atom may be shared between two adjacent clusters, enhancing the structural order of the second-nearest-neighbors of both clusters. [We note that the characteristic length scale of two adjacent clusters ($\approx$15 Å) agrees well with the distance over which enhanced structural order is observable in the RRDF's.] Such a model would explain why a relatively small amount of added Ta can significantly affect the medium-range order of the amorphous alloy, but not be enough to measurably affect the atomic density.

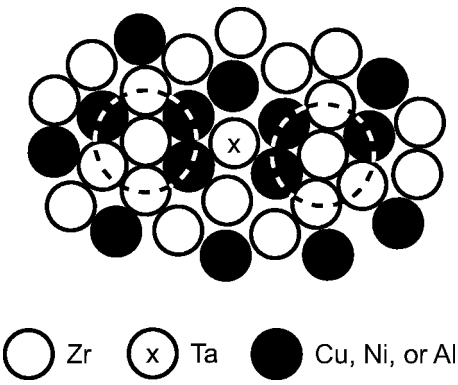

FIG. 6. Effect of Ta on the second-nearest-neighbor environment around Zr atoms. The first-nearest-neighbor shells around two Zr atoms are indicated by dashed lines. Ta is coordinated primarily by Ni and Al and enhances the second-nearest-neighbor shell of two adjacent clusters.

Additional experiments will be required to verify this picture. In particular, fluctuation microscopy could shed some light on the medium-range order. Also, x-ray absorption spectroscopy could reveal details of the short-range order around Ta atoms and, in particular, whether there are any Ta-Ta near neighbors (which would not be predicted to exist based on our model). We have performed some anomalous scattering experiments at the Ta L_{III} edge in an effort to learn more, but the results were inconclusive due to the low concentration of Ta in these alloys.

It is interesting to speculate what effect the differences in structure we observe here may have on the mechanical properties of these amorphous alloys. Based on the changes in the medium-range order, it seems clear that the addition of Ta somehow affects the distribution of free volume in the amorphous structure. In particular, given that the differences in short-range order (particularly around Zr atoms) are small, it appears that Ta may change how free volume is distributed in the regions between the short-range order clusters. (The overall level of free volume is apparently unaffected by the

presence of Ta.) The free volume distribution may, in turn, affect the initiation and propagation of shear bands. A more detailed understanding of these effects will require the development of more detailed models of the micromechanisms of deformation in amorphous alloys.

V. CONCLUSIONS

By using resonant x-ray scattering, we have examined the effect of Ta on the structure of $(Zr_{70}Cu_{20}Ni_{10})_{90-x}Ta_xAl_{10}$ amorphous alloys. Taking advantage of the ability of x-ray scattering to accurately sample reciprocal space at smaller q than is possible with x-ray absorption spectroscopy, we find that Ta has little effect on the nearest-neighbor environment around Zr atoms, but does significantly enhance the order in the second-nearest-neighbor atomic shell. This enhanced structural order persists out to distances of $\sim$15 Å. The addition of Ta also increases the atomic density of the alloy, but this is primarily due to the fact that the Ta atoms are smaller than the Zr atoms they replace. We propose that the effect of Ta may be to create stronger topological ordering between adjacent atomic clusters in the alloy.

ACKNOWLEDGMENTS

We gratefully acknowledge C. Fan for preparing the samples used in this work, H. Ishii for assistance with the x-ray scattering experiments, and R. H. Pratt and L. Kissel for useful discussions relating to the angular dependence of the anomalous scattering factors. This research was supported by the National Science Foundation under Grant No. 9875115. Portions of this research were carried out at the Stanford Synchrotron Radiation Laboratory, a national user facility operated by Stanford University on behalf of the U.S. Department of Energy, Office of Basic Energy Sciences.

*Electronic address: hufnagel@jhu.edu

[1] A. Inoue, Acta Mater. **48**, 279 (2000).
[2] W.L. Johnson, JOM **54**, 40 (2002).
[3] H.A. Bruck, T. Christman, A.J. Rosakis, and W.L. Johnson, Scr. Metall. Mater. **30**, 429 (1994).
[4] H. Chen, Y. He, G.J. Shiflet, and S.J. Poon, Nature (London) **367**, 541, (1994).
[5] H.A. Bruck, A.J. Rosakis, and W.L. Johnson, J. Mater. Res. **11**, 503 (1996).
[6] R.D. Conner, A.J. Rosakis, W.L. Johnson, and D.M. Owen, Scr. Mater. **37**, 1373 (1997).
[7] C.J. Gilbert, R.O. Ritchie, and W.L. Johnson, Appl. Phys. Lett. **71**, 476 (1997).
[8] C.T. Liu, L. Heatherly, D.S. Easton, C.A. Carmichael, J.H. Schneibel, C.H. Chen, J.L. Wright, M.H. Yoo, J.A. Horton, and A. Inoue, Metall. Mater. Trans. A **29**, 1811 (1998).
[9] P. Lowhaphandu and J.J. Lewandowski, Scr. Mater. **38**, 1811 (1998).
[10] K.M. Flores and R.H. Dauskardt, Scr. Mater. **41**, 937 (1999).
[11] K.M. Flores and R.H. Dauskardt, J. Mater. Res. **14**, 638 (1999).
[12] P. Lowhaphandu, S.L. Montgomery, and J.J. Lewandowski, Scr. Mater. **41**, 19 (1999).
[13] T.C. Hufnagel, T. Jiao, Y. Li, L.-Q. Xing, Y. Li, and K.T. Ramesh, J. Mater. Res. **17**, 1441 (2002).
[14] P.M. Voyles, J.M. Gibson, and M.M.J. Treacy, J. Electron Microsc. **49**, 259 (2000).
[15] J. Li, X. Gu, and T. C. Hufnagel, Microsc. Microanal. (to be published).
[16] M. Guerdane and H. Teichler, Phys. Rev. B **65**, 014203 (2002).
[17] L.-Q. Xing, Y. Li, K.T. Ramesh, J. Li, and T.C. Hufnagel, Phys. Rev. B **64**, 180201(R) (2001).
[18] H. Ishii, Ph.D. dissertation, Stanford University, 2002.
[19] C.N.J. Wagner, J. Non-Cryst. Solids **31**, 1 (1978).
[20] N. Norman, Acta Crystallogr. **10**, 370 (1957).
[21] J. Krogh-Moe, Acta Crystallogr. **9**, 951 (1956).
[22] L. Kissel, B. Zhou, S.C. Roy, S.K. Sen Gupta, and R.H. Pratt, Acta Crystallogr., Sect. A: Found. Crystallogr. **51**, 271 (1995).
[23] L. Kissel, Indian J. Phys. **71B**, 309 (1997).
[24] D.T. Cromer and D. Liberman, J. Chem. Phys. **53**, 1891 (1970).
[25] B.L. Henke, E.M. Gullikson, and J.C. Davis, At. Data Nucl. Data Tables **54**, 181 (1993).
[26] J.J. Hoyt, D. de Fontaine, and W.K. Warburton, J. Appl. Crystallogr. **17**, 344 (1984).
[27] P.M. Bergstrom, Jr., L. Kissel, R.H. Pratt, and A. Costescu, Acta Crystallogr., Sect. A: Found. Crystallogr. **53**, 7 (1997).
[28] A. Costescu, P.M. Bergstrom, Jr., C. Dinu, and R.H. Pratt, Phys. Rev. A **50**, 1390 (1994).
[29] E. Matsubara, T. Tamura, Y. Waseda, A. Inoue, T. Zhang, and T. Masumoto, Mater. Trans., JIM **33**, 873 (1992).
[30] E. Matsubara and Y. Waseda, Mater. Trans., JIM **36**, 883 (1995).
[31] J.C. Slater, J. Chem. Phys. **41**, 3199 (1964).
[32] N.J. Shevchik, Philos. Mag. **35**, 805 (1977).
[33] P.H. Fuoss, P. Eisenberger, W.K. Warburton, and A. Bienenstock, Phys. Rev. Lett. **46**, 1537 (1981).
[34] E. Matsubara, M. Sakurai, T. Nakamura, M. Imafuku, S. Sato, J. Saida, and A. Inoue, Scr. Mater. **44**, 2297 (2001).
[35] G.S. Cargill III, Solid State Phys. **30**, 227 (1975).
[36] P. H. Gaskell, in *Glasses and Amorphous Materials*, edited by R. W. Cahn, P. Haasen, and E. J. Kramer, volume 9 of *Materials Science and Technology: A Comprehensive Treatment* (VCH, Weinheim, 1991), Chap. 4.
[37] C.L. Briant and J.J. Burton, Phys. Status Solidi B **85**, 393 (1978).